



## Antibacterial properties of photo-crosslinked chitosan/methacrylated hyaluronic acid nanoparticles loaded with bacitracin

Raquel R. Gonçalves<sup>a,b,c</sup>, Daniela Peixoto<sup>a,b</sup>, Rui R. Costa<sup>a,b</sup>, Albina R. Franco<sup>a,b</sup>, Vânia I.B. Castro<sup>a,b</sup>, Ricardo A. Pires<sup>a,b</sup>, Rui L. Reis<sup>a,b</sup>, Iva Pashkuleva<sup>a,b</sup>, Devid Maniglio<sup>c</sup>, Annalisa Tirella<sup>c</sup>, Antonella Motta<sup>c</sup>, Natália M. Alves<sup>a,b,\*</sup>

<sup>a</sup> 3B's Research Group, I3Bs – Research Institute on Biomaterials, Biodegradables and Biomimetics, University of Minho, Headquarters of the European Institute of Excellence on Tissue Engineering and Regenerative Medicine, AvePark, Parque de Ciência e Tecnologia, Zona Industrial da Gandra, 4805-017 Barco, Guimarães, Portugal

<sup>b</sup> ICV3S/3B's-PT Government Associate Laboratory, Braga/Guimarães, Portugal

<sup>c</sup> BIOTech Research Center, Department of Industrial Engineering, University of Trento, Via Delle Regole 101, 38123 Trento, Italy

### ARTICLE INFO

#### Keywords:

Nanoparticles  
Methacrylated hyaluronic acid  
Photo-crosslinking  
Bacitracin  
Chronic wounds

### ABSTRACT

The current treatments for wounds often fail to induce adequate healing, leaving wounds vulnerable to persistent infections and development of drug-resistant microbial biofilms. New natural-derived nanoparticles were studied to impair bacteria colonization and hinder the formation of biofilms in wounds. The nanoparticles were fabricated through polyelectrolyte complexation of chitosan (CS, polycation) and hyaluronic acid (HA, polyanion). UV-induced photo-crosslinking was used to enhance the stability of the nanoparticles. To achieve this, HA was methacrylated (HAMA, degree of modification of 20 %). Photo-crosslinked nanoparticles obtained from HAMA and CS had a diameter of 478 nm and a more homogeneous size distribution than nanoparticles assembled solely through complexation (742 nm). The nanoparticles were loaded with the antimicrobial agent bacitracin (BC), resulting in nanoparticles with a diameter of 332 nm. The encapsulation of BC was highly efficient (97 %). The BC-loaded nanoparticles showed significant antibacterial activity against gram-positive bacteria *Staphylococcus aureus*, *Methicillin-resistant S. aureus* and *S. epidermidis*. Photo-crosslinked HAMA/CS nanoparticles loaded with BC demonstrated inhibition of biofilm formation and a positive effect on the proliferation of mammalian cells (L929). These crosslinked nanoparticles have potential for the long-term treatment of wounds and controlled antibiotic delivery at the location of a lesion.

### 1. Introduction

Wound healing is the natural physiological response that occurs when a tissue recovers from damage a complex process that involves hemostasis, inflammation, proliferation, and remodeling [1,2]. Some wounds are characterized by a full-thickness depth, excessive inflammatory response, and slow healing, becoming chronic wounds or ulcers. When wounds do not heal in a timely manner, they often develop persistent infections and form drug-resistant microbial biofilms [3]. Their development is linked to underlying conditions such as ischemia, diabetes, venous stasis disease, obesity, and age [4,5]. Current wound healing treatments used in clinics are based on prevention and early

detection. After diagnosis, the adopted measures include cleansing and debridement, infection and inflammation control, pressure redistribution, restoration of tissue perfusion measures, and advanced cell therapies. These approaches can be used alone or can be combined to boost the healing process [6–8]. Nonetheless, the treatment can fail to completely close the ulcers, which is solved by amputations and results in a lower quality of life for patients, and in some cases, even death [9,10]. Such poor clinical outcomes demonstrate that new treatments and devices are needed to improve the healing process.

Nanomaterials are a promising tool to enhance the wound healing. Numerous studies have shown that nanoparticles improve stability, cross-membrane transport, circulation time, safety, and are efficient in

\* Corresponding author at: 3B's Research Group, I3Bs – Research Institute on Biomaterials, Biodegradables and Biomimetics, University of Minho, Headquarters of the European Institute of Excellence on Tissue Engineering and Regenerative Medicine, AvePark, Parque de Ciência e Tecnologia, Zona Industrial da Gandra, 4805-017 Barco, Guimarães, Portugal.

E-mail address: [nalves@i3bs.uminho.pt](mailto:nalves@i3bs.uminho.pt) (N.M. Alves).

<https://doi.org/10.1016/j.ijbiomac.2024.134250>

Received 15 March 2024; Received in revised form 25 July 2024; Accepted 27 July 2024

Available online 30 July 2024

0141-8130/© 2024 The Authors. Published by Elsevier B.V. This is an open access article under the CC BY license (<http://creativecommons.org/licenses/by/4.0/>).

encapsulating drugs, such as antibiotics [11–13]. Nanoparticulate systems can be readily produced from charged biomacromolecules via electrostatic interactions. For example, chitosan (CS) and hyaluronic acid (HA) are common polyelectrolytes used to generate nanocomplexes [14]. CS is a linear polycation widely used in drug delivery and in wound dressings [15,16] due to its antibacterial properties [17] and ability to modulate inflammatory processes [18]. HA is a linear polyanionic glycosaminoglycan involved in the homeostasis of tissue hydration and the remodeling of the extracellular matrix (ECM) following injury [19,20]. Previous studies have shown that CS and HA generate feasible and versatile systems for an efficient delivery of bioactive substances. For example, Parajó et al. demonstrated the efficiency of CS/HA nanoparticles in delivering pro-angiogenic growth factors [21], whereas Tirella et al. showed their ability for siRNA delivery [22]. Similarly, Lallana et al. showed that larger negatively charged RNA can be loaded into CS/HA nanoparticles [23]. Yang et al. further showcased that CS/HA nanoparticles can also serve as nanovehicles for water-insoluble substances such as curcuminoid [24]. In the study by Lima et al., functionalized CS/HA nanoparticles demonstrated successful internalization under normal and pro-inflammatory states in primary human articular chondrocytes, as well as in human umbilical vein endothelial cells, and human monocytes [25].

Because of their physicochemical characteristics, nanoscale size, and ease of the complexation reaction, CS and HA offer specific benefits in wound treatment. Moreover, these biomaterials can be chemically modified with functional groups to enhance the potential of the cross-linked constructs for wound healing by increasing the crosslinking density and colloidal stability [26,27]. In this study, we used polyelectrolyte complexation to produce nanoparticles based on CS and a methacrylate-modified HA (HAMA) to make it UV photo-crosslinkable. Photo-crosslinking method can tune the mechanical properties and drug loading capacity while maintaining biocompatibility [28,29]. As an example, photo-crosslinking applied to particulate systems has improved the loading and delivery of gene-based therapeutics from acrylate-derived nanoparticle matrices [26,30].

On the other hand, the photo-crosslinking post-treatment can affect the size, uniformity, and stability of the complex nanoparticles [31]. Herein, HAMA/CS were developed using photo-crosslinking the ability of the developed nanoparticles to serve as drug vehicles is demonstrated by the encapsulation of bacitracin, a cyclic polypeptide antibiotic effective against gram-positive bacteria used for the short-term prevention and treatment of infections [32]. The antibacterial efficacy of BC-loaded NPs against bacteria responsible for wound infections was showcased, indicating a potential in treatment of acute and chronic skin infections.

## 2. Materials and methods

### 2.1. Materials

Dried Sodium Hyaluronate (HA) (molecular weight: 151–300 kDa) was purchased from LifeCore. Chitosan (CS) (low molecular weight: 50–190 kDa,  $\geq 75.0\%$  deacetylation), bacitracin zinc salt (from *Bacillus licheniformis*,  $\sim 70,000$  U/g), methacrylic anhydride (MA, topanol A 2.000 ppm inhibitor, 94 %), lithium phenyl-2,4,6-trimethylbenzoylphosphinate photoinitiator (LAP, purity  $\geq 95\%$ ), and PBS tablets were purchased from Sigma-Aldrich. Membranes Spectra/Por 3, cut-off 3.5 kDa were purchased from Fisher Scientific. Hydrochloric acid (HCl) was purchased from Honeywell. Sodium hydroxide (NaOH) was purchased from Panreac. Mueller-Hinton (MH) agar and Tryptic Soy (TS) Broth were purchased from Neo Biotech.

### 2.2. Synthesis of methacrylated hyaluronic acid

Methacrylated HA (HAMA) was synthesized using an adapted protocol from Loebe et al. [33]. Briefly, a solution of 6 mg/mL HA was

prepared in ultra-pure water and left stirring overnight. The solution was placed in an ice bath and the pH was adjusted to 8.5 by dropwise addition of 1 M NaOH under stirring. The methacrylation was performed by the slow addition of methacrylic anhydride to the HA solution (1.5 mL per gram of HA) at pH 8.5 (pH continuously adjusted with 5 M NaOH). The reaction was carried overnight at room temperature and finally, the pH was readjusted to 8.5. Unreacted chemicals were removed by dialysis (membranes Spectra/Por 3, cut-off 3.5 kDa) against osmotized water (OW). The final product was lyophilized and stored at  $-20\text{ }^{\circ}\text{C}$ . The success of the modification was confirmed by  $^1\text{H}$  NMR (Bruker Avance, 400 MHz) and the spectra were integrated to calculate the degree of the substitution.

### 2.3. Preparation of nanoparticles based on chitosan and hyaluronic acid

Nanoparticles were produced following a protocol adapted from Tirella et al. [22] and Lallana et al. [34]. Briefly, a CS solution was prepared at a concentration of 0.69 mg/mL in HCl (4.6 mM). HA (1.67 mg/mL), HAMA (1.67 mg/mL), and LAP (3.75 mg/mL) solutions were prepared in OW (pH = 5). All solutions were stirred gently overnight followed by an adjustment of the pH to 5 using NaOH (0.1 M) and HCl (0.1 M). CS (250  $\mu\text{L}$ ) was diluted in an equal volume of OW (20 min at 1000 rpm). The resulting 500  $\mu\text{L}$  solution was gently poured into an equal volume of HA or HAMA to obtain HA/CS or HAMA/CS with a mass ratio of 31/100. To obtain photo-crosslinked nanoparticles, LAP was also added to the HAMA solution at a HAMA:LAP volume ratio of 9:1, to initiate the photopolymerization. The mixture was stirred for 30 min at room temperature. The cross-linking of HAMA/CS nanoparticles was made by UV irradiation with a UV lamp (Model Triwood 6/36,  $\lambda = 352$  nm,  $P = 6$  W) for 1 min. Three different formulations were prepared: HA/CS, HAMA/CS and crosslinked HAMA/CS (HAMA/CS-Xlinked).

### 2.4. Characterization of nanoparticles

The hydrodynamic diameter and zeta potential of the obtained nanoparticles were determined by dynamic light scattering (DLS) using a Malvern Nano-ZS zeta-sizer and the Zetasizer Nano v7.19 software. Aliquots of 1 mL were loaded in polystyrene disposable cuvettes and size distribution, z-average and polydispersity index (PDI) were determined. The samples were prepared to ensure a count rate between 250 and 400 kcps. Zeta potential measurements were performed using folded capillary cells. All measurements were made in triplicates.

The morphology of the nanoparticles was analyzed by scanning electron microscopy (SEM, JSM-6010 LV, JEOL). Samples were prepared by centrifuging the nanoparticles suspension at 10000 rpm, discarding the supernatant, and lyophilization. The dry nanoparticles were immobilized on carbon tape and sputtered with platinum.

### 2.5. Nanoparticle stability

The nanoparticles were suspended in 1 mL of OW at 25 and 37  $^{\circ}\text{C}$  for 0, 3, 7 and 14 days. After these periods, the size distribution, z-average, and PDI were measured as above described. The data is presented as averaged results from three independent experiments.

### 2.6. Encapsulation of bacitracin in crosslinked nanoparticles (BC-loaded HAMA/CS-Xlinked nanoparticles)

BC was loaded in HAMA/CS-Xlinked nanoparticles using an adapted protocol of Tirella et al. [22] and Lallana et al. [34]. First, BC was dissolved in OW at a concentration of 0.42 mg/mL (Fig. S3) [35]. This solution was added to an equal volume of CS at 0.69 mg/mL and they were mixed for 20 min at 1000 rpm. 500  $\mu\text{L}$  of the resulting mixture was poured into an equal volume of the HAMA/LAP solution (as described in Section 2.3). After 30 min, the NPs were irradiated with a UV lamp (Model Triwood 6/36,  $\lambda = 352$  nm) for 1 min. The loaded nanoparticles

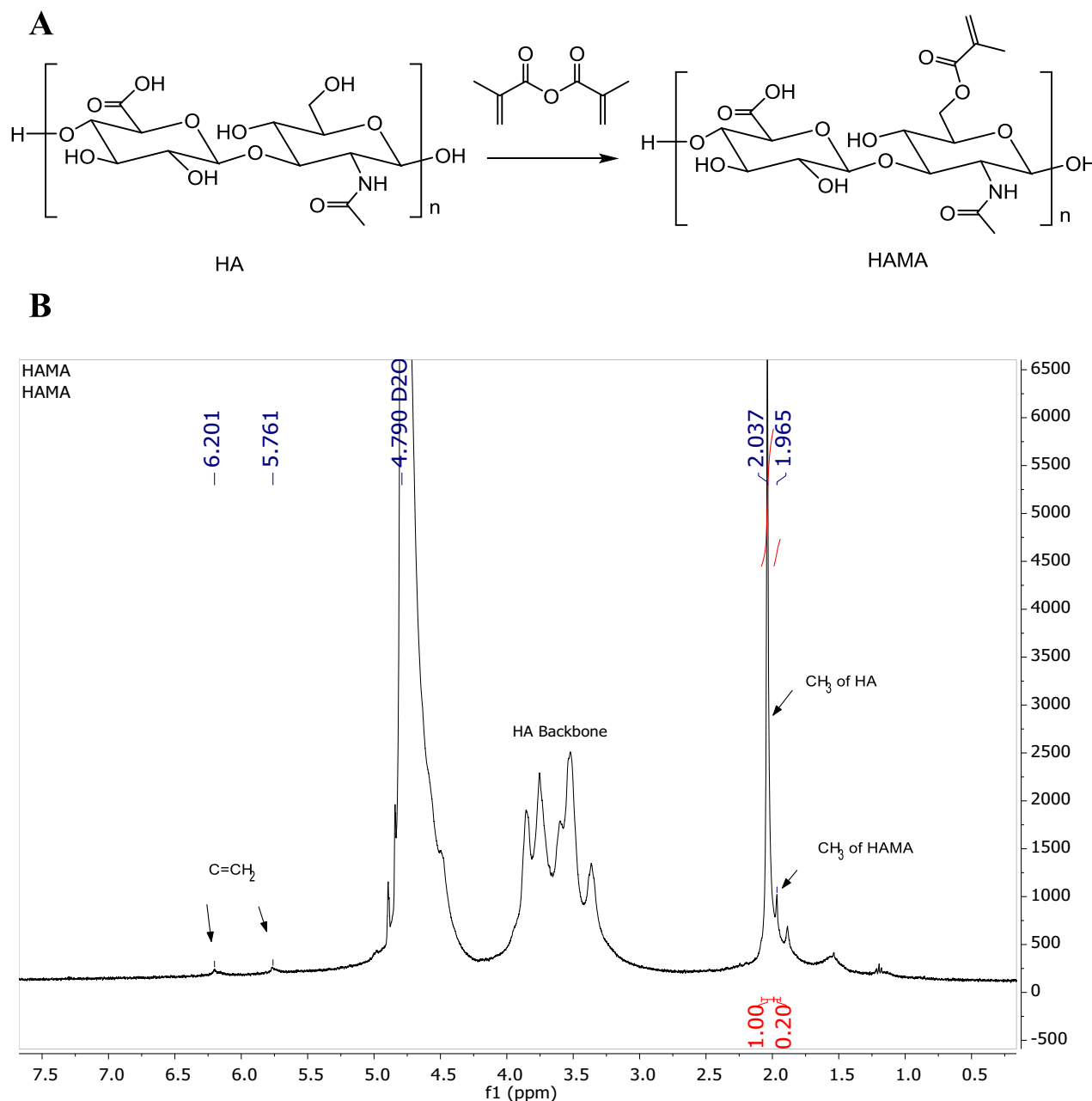


**Fig. 1.** (A) Schematic presentation of the chemical reaction used for the methacrylation of hyaluronic acid (HA) and (B)  $^1\text{H}$  NMR spectrum of the obtained methacrylated hyaluronic acid (HAMA).

were characterized by DLS and SEM. The BC encapsulation efficiency was determined by analytical High-Performance Liquid Chromatography (HPLC, Alliance, Waters Corporation, USA) using a C18 Atlantis column (250 mm  $\times$  4.6 mm, 5  $\mu\text{m}$ , Waters Corporation, USA). The samples were passed through a 0.22  $\mu\text{m}$  pore size filter and 10  $\mu\text{L}$  were injected. The isocratic method was applied using Phosphate buffer 0.5 M and methanol (30:70) at a flow rate of 1 mL/min [36]. The detection wavelength was performed at 254 nm and the elution time was 30 min.

## 2.7. Antibacterial activity of BC-loaded HAMA/CS-Xlinked nanoparticles

### 2.7.1. Radial diffusion assay

The antibacterial activity of BC-loaded HAMA/CS-Xlinked nanoparticles was evaluated against different well-known wound infecting Gram-positive pathogens [37], namely *Staphylococcus aureus* ATCC 25923 (*S. aureus*), Methicillin-resistant *S. aureus* ATCC 700698 (MRSA)

and *Staphylococcus epidermidis* ATCC 12228 (*S. epidermidis*). Unloaded nanoparticles and free BC in solution (7  $\mu\text{g}/\text{mL}$ ; Fig. S3) were used as controls. First, the minimal inhibitory concentration of BC was evaluated using the Kirby-Bauer disc diffusion method for testing microbial susceptibility to new antibiotic drugs [38]. Briefly, the bacterial cultures were grown overnight at 37  $^\circ\text{C}$  with agitation (140 rpm), and their optical density was adjusted to 0.1 ( $\lambda = 610$  nm; McFarland standard 0.5) to obtain a bacterial inoculum of  $10^8$  CF/mL. They were spread on Muller Hinton Agar (Oxoid, UK) with a sterile swab. Blank discs were impregnated with 30  $\mu\text{L}$  of each BC solution (0.052, 0.104, 0.208, 0.500, and 0.800 mg/mL). The concentrations of BC were chosen according to the literature available [39]. Negative controls with sterile PBS were used. The plates were incubated for 16 h at 37  $^\circ\text{C}$ . The area of growth inhibition was calculated by measuring the diameter of the halo formed around the disks.

The agar well diffusion method was employed as an adaptation of the

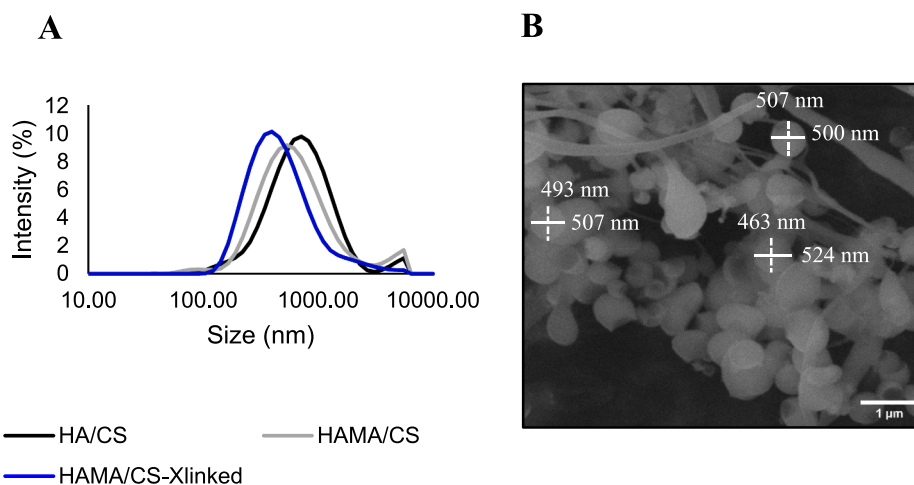


**Fig. 2.** (A) Dynamic light scattering (DLS) data showing the size distribution on nanoparticle samples. Representative spectra are represented. Peaks around 10,000 nm are attributed to NP aggregates (low signal,  $\approx 1$  % intensity). (B) Representative scanning electron microscopy image of crosslinked nanoparticles.

**Table 1**

DLS data for size, polydispersity and charge of the obtained nanoparticles.

Formulation	Size (nm)	PDI	Zeta potential (mV)
HA/CS	769 $\pm$ 69	0.373 $\pm$ 0.068	-35.8 $\pm$ 0.2
HAMA/CS	742 $\pm$ 231	0.410 $\pm$ 0.054	-32.5 $\pm$ 0.6
HAMA/CS-Xlinked	478 $\pm$ 86	0.300 $\pm$ 0.074	-29.2 $\pm$ 1.1

Kirby-Bauer disc diffusion technique for testing microbial susceptibility to new nanoparticles [38]. This method provides a more reliable assessment of charged substances, which can adhere to the hydrophilic surface of the disc and do not disperse into the surrounding medium [40–42]. The bacterial cultures were grown as described above and their optical density was adjusted to 0.1 ( $\lambda = 610$  nm; McFarland standard 0.5) corresponding to a bacterial inoculum of  $10^8$  CFU/mL. They were then spread onto Muller Hinton Agar (Oxoid, UK) with a sterile swab. Four wells (4 mm diameter) were made with a sterile punch and 30  $\mu$ L of each nanoparticle suspension was added per well [40–42]. Negative control with PBS and positive control with BC solution were used. The plates were incubated for 48 h at 25  $^{\circ}$ C and for 16 h at 37  $^{\circ}$ C. The growth inhibition was determined by measuring the diameter of the halo formed around the disks [43,44]. All experiments were performed in triplicates to ensure reproducibility.

### 2.7.2. Bacterial viability in liquid media

The viability of Gram-positive bacteria in the presence of the BC-loaded HAMA/CS-Xlinked nanoparticles was assessed against *S. aureus*, MRSA, and *S. epidermidis* [45]. All the nanoparticles were produced in sterile conditions. Bacterial cultures were grown overnight in Tryptone Soya Broth (TSB; Oxoid, UK) medium at 37  $^{\circ}$ C overnight with agitation (150 rpm) and adjusted to an optical density of 0.1 ( $\lambda = 610$  nm). A volume of 60  $\mu$ L of the bacterial suspensions was added to 60  $\mu$ L of 2 x concentrated HAMA/CS-Xlinked nanoparticles and BC-loaded HAMA/CS-Xlinked nanoparticles. 60  $\mu$ L of BC solution (0.7 mg/mL) was used as positive control and 60  $\mu$ L of sterile PBS as negative control. Samples were incubated at 37  $^{\circ}$ C under static conditions for 24 h and 72 h. After each timepoint, serial dilutions were made, spread onto Tryptone Soya Agar (TSA; Oxoid, UK), and incubated overnight at 37  $^{\circ}$ C. The bacterial viability was determined as the log the colony forming units (CFU/mL). Each experiment was performed in triplicate at two timepoints.

### 2.8. Antibiofilm activity of the BC-Loaded HAMA/CS-Xlinked nanoparticles

The antibiofilm activity of the BC-loaded HAMA/CS-Xlinked nanoparticles was assessed against *S. aureus*, MRSA, and *S. epidermidis* using the microtiter plate method according to Haney et al. [46]. A bacterial biofilm was first established for all the strains in 96-well plates. Bacterial cultures were grown overnight in TSB medium at 37  $^{\circ}$ C with agitation (150 rpm) and 100  $\mu$ L of each bacterial suspension adjusted to an optical density of 0.1 ( $\lambda = 610$  nm) was added to the 96-well plate and incubated for 16 h at 37  $^{\circ}$ C under static conditions. After incubation, the adhered biofilms were gently rinsed with sterile PBS, followed by aspirator of the rinsing media. Then, 60  $\mu$ L of 2 x concentrated solution of HAMA/CS-Xlinked nanoparticles, BC-loaded HAMA/CS-Xlinked nanoparticles, BC in solution or sterile TSB were added in triplicate to each well containing the biofilm. Plates were incubated at 37  $^{\circ}$ C for 24 h and 72 h under static conditions. The bacterial recoverable from the biofilm after each treatment was determined as the log the colony forming units (CFU/mL). As for biofilm formation, it was quantified using Crystal Violet method [46]. Briefly, after incubation, 96-well plates were washed with sterile PBS three times to remove planktonic bacteria and leave plate to dry. Then, adherent bacterial cells were fixed with 100 % methanol for 20 min and stained with crystal violet (0.1 % w/v) for 20 min. Afterwards, each well was washed twice with PBS, and bound crystal violet was released by adding 33 % (vol/vol) acetic acid. The OD of the resulting solution was measured at 595 nm using a microplate reader (BIO-TEK instruments). Each experiment was performed in triplicate at two timepoints.

### 2.9. Biological assays

*In vitro* cellular tests of the HAMA/CS-Xlinked and BC-loaded HAMA/CS-Xlinked nanoparticles were performed using L929 mouse fibroblast cells cultured in DMEM supplemented with 10 % of fetal bovine serum (FBS) and 1 % of Antibiotic-Antimycotic solution [47–49]. The cells were grown in a T150 flask and incubated at 37  $^{\circ}$ C in a humidified air atmosphere of 5 % CO<sub>2</sub>. When 80 % of confluence was reached, the cells were washed with Dulbecco's Phosphate-Buffered Saline (DPBS) and subsequently detached with 5 mL of trypLE™ express solution for 5 min at 37  $^{\circ}$ C. To inactivate the trypLE™ express solution effect, 10 mL of DMEM was added. The cells were centrifuged at 300 xg for 5 min and the medium was removed. The pellet was resuspended in DMEM. Cellular seeding was performed in nanoparticles produced at sterile conditions and suspended in DMEM. 20  $\mu$ L of supplemented DMEM containing also a cell suspension with a density of

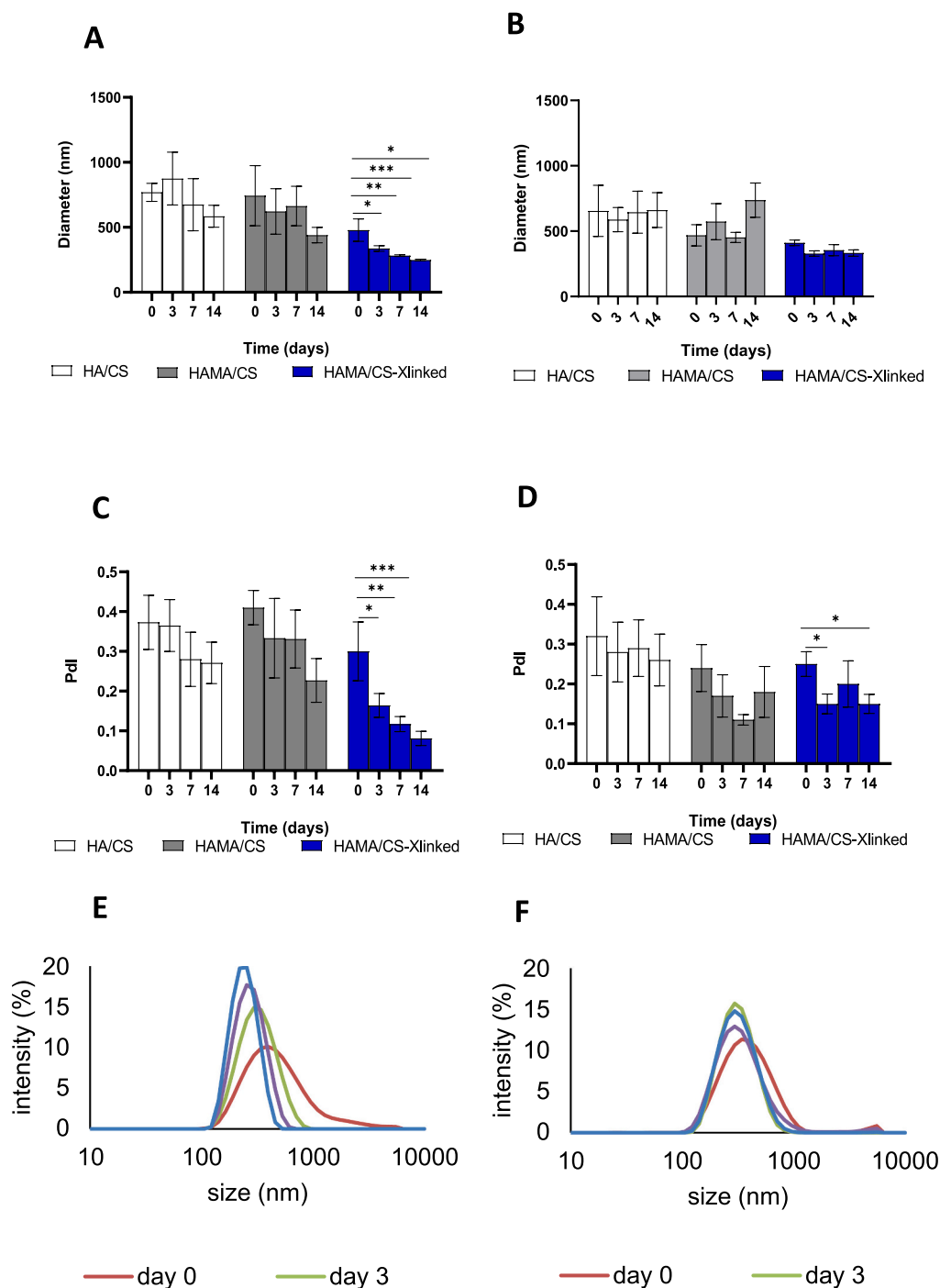


**Fig. 3.** Dynamic light scattering (DLS) data showing the size variations of nanoparticles samples at 25 °C (A) and 37 °C (B). PDI variations of nanoparticles samples at 25 °C (C) and 37 °C (D). Size distribution evolution of HAMA/CS-Xlinked nanoparticles at 25 °C (E) and 37 °C (F).

30,000 cells was added dropwise with the culture plate and incubated at 37 °C in a humidified air atmosphere of 5 % CO<sub>2</sub>. Tissue culture polystyrene (TCPS) seeding only with cells was used as positive control. All experiments were performed in triplicate.

The metabolic activity of L929 cells treated with HAMA/CS-Xlinked and BC-loaded HAMA/CS-Xlinked nanoparticles were determined using the Alamar-Blue assay [47–49]. After 1 and 3 days of culture, the culture medium was removed and the cells were washed twice with sterile PBS (pH 7.4). Then, fresh DMEM supplemented with 10 % of Alamar-blue reagent (Xpert Blue Cell Viability Assay, GRISP) was added to each well, followed by incubation at dark for 4 h at 37 °C in a humidified air

atmosphere of 5 % CO<sub>2</sub>. Afterwards, 100 µL of each solution was transferred to a 96-well black plate and the absorbance was measured at 570 nm excitation wavelength and at 600 nm emission wavelength as a reference control, using a microplate reader (BIO-TEK instruments). The experiments were run in triplicate.

Cell proliferation was evaluated by dsDNA picogreen quantification (P11495, Invitrogen), according to the manufacturer's instructions [47–49]. After each incubation time, DMEM was removed from each well and the cells were washed twice with sterile PBS (pH 7.4). Then, 1 mL of ultrapure water was added to each well to induce complete membrane lysis, incubated at 37 °C for 1 h and stored at –80 °C until



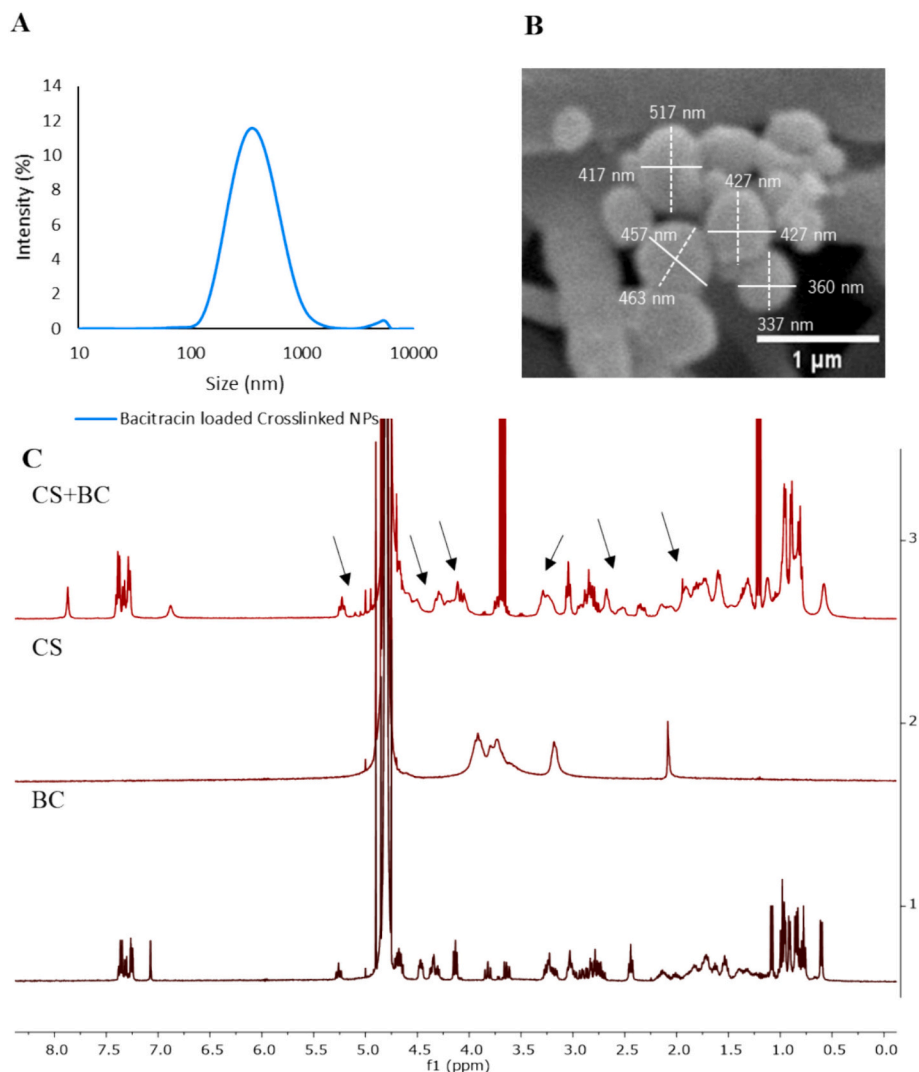


Fig. 4. (A) Size distribution on BC-loaded HAMA/CS-Xlinked nanoparticles. (B) SEM imaging of BC-loaded HAMA/CS-Xlinked nanoparticles, with diameter measurements. (C) <sup>1</sup>H NMR spectra (400 MHz, D<sub>2</sub>O) of BC, CS, and CS + BC.

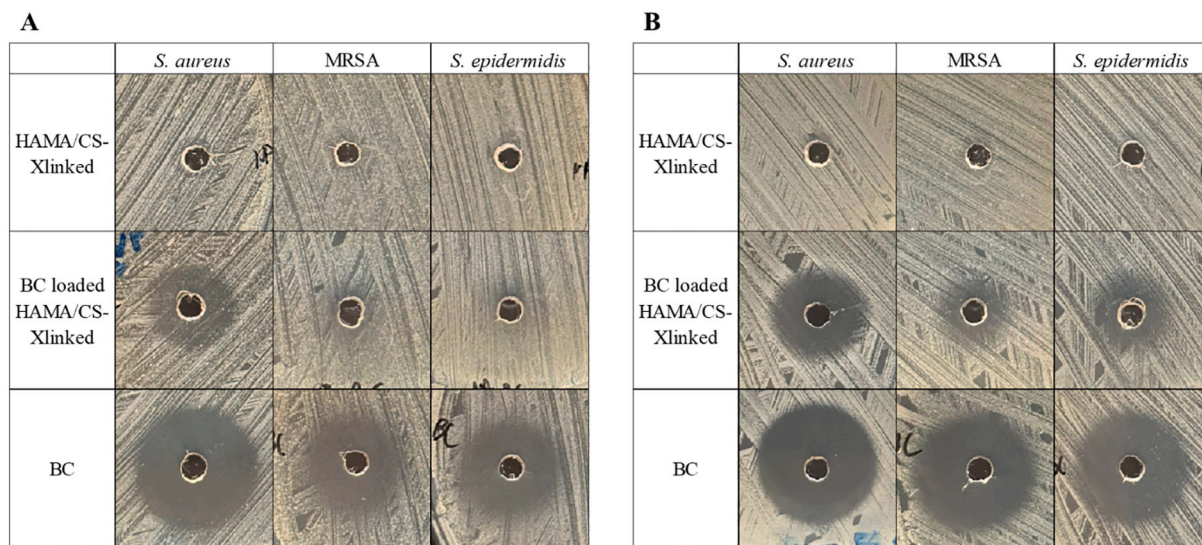


Fig. 5. Representative images showing of the antibacterial activity of HAMA/CS-Xlinked nanoparticles, BC-loaded HAMA/CS-Xlinked nanoparticles, and BC against *S. aureus*, MRSA, *S. epidermidis* using agar well diffusion assay at 25 °C (A) and 37 °C (B).

**Table 2**

Qualitative data (diameter of inhibition zones) about the antibacterial effect of different formulations.

Temperature	Formulation	Diameter of the inhibition zone [mm]		
		<i>S. aureus</i>	MRSA	<i>S. epidermidis</i>
25 °C	HAMA/CS-Xlinked	0	0	0
	BC-loaded HAMA/CS-Xlinked	14	5	5
	BC	20	16	17
37 °C	HAMA/CS-Xlinked	0	0	0
	BC-loaded HAMA/CS-Xlinked	15	11	11
	BC	19	19	19

further analysis. After thawing, samples were analyzed for DNA content and measured at an excitation wavelength of 485/20 nm and at an emission wavelength of 528/20 nm. DNA content was calculated according to a standard curve. The experiments were run in triplicate.

The cell viability of L929 cells treated with HAMA/CS-Xlinked and BC-loaded HAMA/CS-Xlinked nanoparticles were determined by live/dead assay (Calcein AM stains the live cells in green and PI stains dead cells in red) [47–49]. After 1 and 3 days of treatment, the culture medium was removed and a fresh medium supplemented with 0.2 % Calcein AM and 0.1 % PI were added to the immersed for 30 min at dark, washed with DPBS, and analyzed using an inverted incubation microscope with Thunder (DMI8, Leica, Germany).

### 2.10. Statistical analysis of the obtained data

All the quantitative results were obtained from triplicate assays. Data are reported as mean  $\pm$  standard deviation and tested for normality. Significant statistical variations were calculated by One-way ANOVA with Tukey tests to compare between more than two groups; and Two-way ANOVA with Bonferroni tests to compare between more than two groups (GraphPad Prism 9, San Diego CA, USA). The levels of significance for statistical differences are presented as  $p < 0.05$  (\*),  $p < 0.01$  (\*\*), and  $p < 0.001$  (\*\*\*)).

## 3. Results and discussion

### 3.1. Synthesis and characterization of HAMA

In order to obtain HAMA, a well-established method of HA methacrylation by reaction with methacrylic anhydride was used (Fig. 1A) [31]. The modification was confirmed by  $^1\text{H}$  NMR (Fig. 1B), which revealed new signals at 5.7 ppm and 6.2 ppm for the protons of vinyl groups, and at 1.9 ppm for the methyl protons (Fig. 1B and Fig. S1) [31]. The degree of methacrylation was 20 %, as calculated from the ratio of the integral of the HA methyl proton peak at 2.0 ppm to the HAMA methyl proton peak at 1.9 ppm (arrows in Fig. 1B).

### 3.2. Assembly and characterization of nanoparticles

The CS and HA used in this study are appealing materials not only because of their benefits in the pharmaceutical industry but also because they exhibit ionizable amine and carboxyl groups, which allow their complexation by electrostatic interactions [50]. The nanoparticles were obtained by mixing CS with HA or HAMA at room temperature. DLS measurements showed that nanoparticles assembled from HA/CS and HAMA/CS have similar diameters of 742 and 769 nm, respectively (Fig. 2A and Table 1). However, they showed high polydispersity ( $\text{PDI} > 0.37$ ) indicating instability and/or aggregation. So, an additional modification via cross-linking was made. HAMA/CS-Xlinked nanoparticles had a smaller diameter (478 nm) and lower polydispersity ( $\text{PDI} = 0.30$ , consistent with a more uniform distribution) [51]. As expected, the nanoparticles were negatively charged due to the non-stoichiometric ratio of the used components, i.e. HA was used in excess compared to CS [52]. The zeta potentials were approximately  $-30$  mV, indicating that the suspended nanoparticles retain colloidal stability [53]. Scanning electron microscopy (SEM) confirmed the data from DLS by showing the formation of nanoparticles with spherical shape (Fig. 2B and Fig. S2).

Different times of UV irradiation, namely 15, 30, 45 and 60 s were tested, but there was no effect on the irradiation time on the size of the nanoparticles (Table S1).

### 3.3. Nanoparticles stability

The stability of nanoparticles is an important factor for their efficacy as a delivery system and is related to the tendency of nanoparticulate formulations to aggregate or degrade overtime [54]. To this end, the

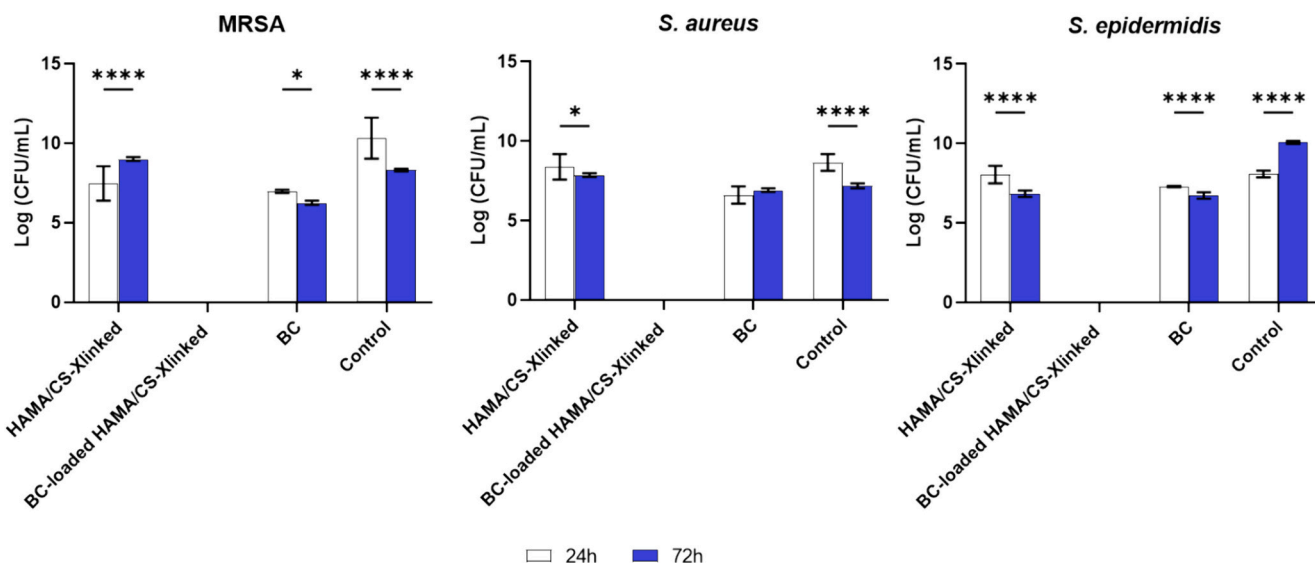


**Fig. 6.** Antibacterial activity of HAMA/CS-Xlinked and BC-loaded HAMA/CS-Xlinked nanoparticles, and BC in solution against *MRSA*, *S. aureus*, and *S. epidermidis* after 24 h and 72 h incubation. Number of recoverable bacteria was evaluated by log (CFU/mL). Control corresponds to the bacteria without any treatment.

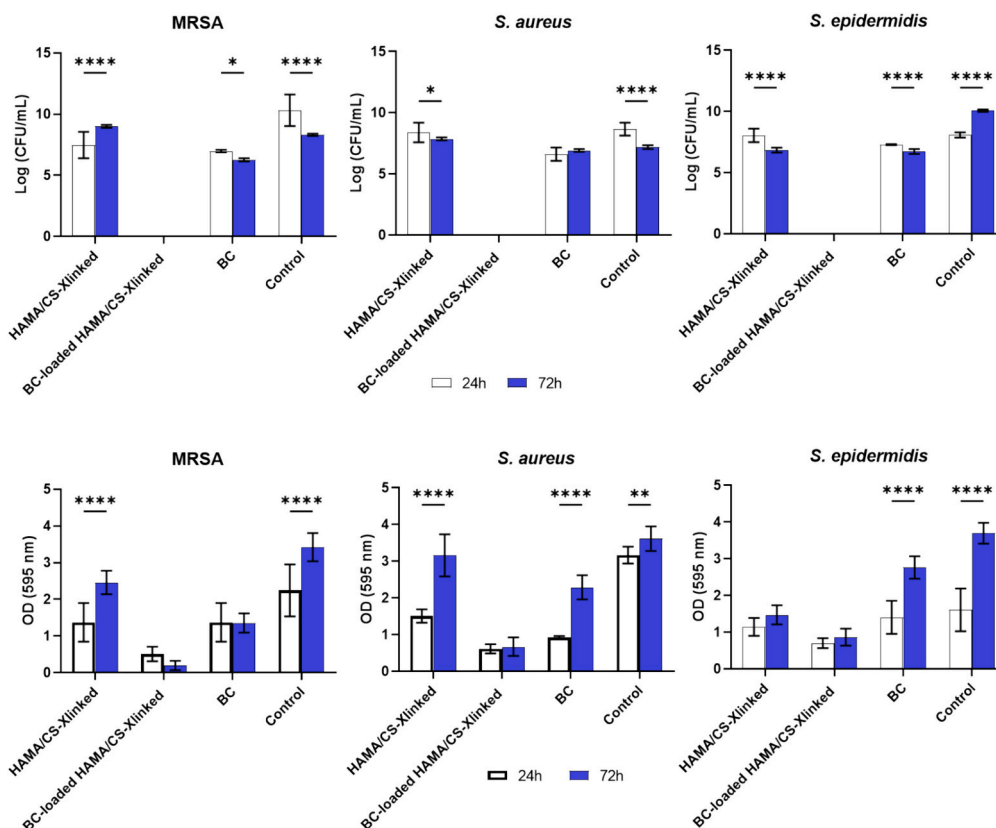


**Fig. 7.** Antibiofilm activity of the HAMA/CS-Xlinked and BC-loaded HAMA/CS-Xlinked nanoparticles, and BC in solution against *MRSA*, *S. aureus*, and *S. epidermidis* after 24 h and 72 h incubation. Control corresponds to the bacteria without any treatment. Biofilm was determined by: (A) Number of recoverable bacteria was evaluated by Log (CFU/mL), and (B) Biofilm biomass formation using the Crystal Violet assay. Significant differences: \*\* $p < 0.01$ , \*\*\*\* $p < 0.0001$ .

hydrodynamic diameters and polydispersity of the different nanoparticles were evaluated during 14 days as an indicator of their stability (Fig. 3). The selected temperatures of 25 °C and 37 °C correspond to the temperature range in which the systems will be used: room temperature (prior application) and physiological temperature (when in contact with the tissue).

Since the pH of chronic wounds is in the range between 7.2 and 8.9 [55], a medium with an acidic pH ( $\approx 5$ ) was chosen. This pH is relevant because an acidic microenvironment reduces the proteolytic activity and bacteria growth that is associated with slow wound healing [56]. In fact, the use of acidic substances has been proposed to accelerate wound healing and restore the acidic pH of the skin milieu [57–59]. HAMA/CS-Xlinked nanoparticles were systematically smaller than HA/CS and HAMA/CS at all time-points as a result of the increased crosslinking density (without crosslinked 769 and 742 nm, respectively and with crosslinked 478 nm). Size is an important aspect to consider when designing drug delivery systems: because particle size is inversely proportional to their diffusion coefficient, smaller particles have higher effective encapsulated doses and are better distributed in tissues [60,61].

Regardless of the composition, at the studied conditions, the size and PDI of HA/CS and HAMA/CS nanoparticles did not change significantly during the studied period of 14 days. The HAMA/CS-Xlinked nanoparticles remained homogenous (*i.e.*,  $PDI < 0.3$ ) and with a diameter below 500 nm but these parameters decreased significantly at 25 °C during the studied period. These data suggest that the crosslinked nanoparticles become more compact over time as the low PDI discards the possibility of nanoparticle fragmentation - an opposite trend would indicate degradation or aggregation [62,63]. At 37 °C, no significant variations of size or PDI were found, indicating nanoparticle stability at these conditions.

### 3.4. Encapsulation of bacitracin

BC, an antibiotic used to treat of wounds, is most effective against gram-positive bacteria [64]. In this study, different concentrations of BC ( $> 0.052$  mg/mL) were tested (Fig. S3 and Table S2). The results show that BC had an inhibitory effect at concentrations  $> 0.5$  mg/mL on all the bacteria tested, which is consistent with previous studies [65]. To endow the HAMA/CS-Xlinked nanoparticles with antibacterial properties, BC was encapsulated at 0.7 mg/mL. The encapsulation efficiency was 97 %, as determined by analytical HPLC (Fig. S4), and it affected the dimensions of this system: the obtained BC-loaded nanoparticles had a diameter of 332 nm (lower than the 478 nm of unloaded HAMA/CS-Xlinked) with a PDI of 0.256 (Fig. 4).

The decrease in the size of BC-loaded HAMA/CS-Xlinked nanoparticles can be explained by the interaction of CS with BC. The  $^1\text{H}$  NMR analysis (Fig. 4C) confirmed a deviation of the CS signals in the presence of more BC, suggesting an interaction between them.

### 3.5. Antibacterial potential of loaded nanoparticles

The antibacterial activity of BC-loaded HAMA/CS-Xlinked nanoparticles was evaluated at 25 and 37 °C against three gram-positive bacteria: *S. aureus*, *MRSA*, and *S. epidermidis* (Fig. 5 and Fig. S5) according to the modified agar-well Kirby–Bauer plate method [35]. Because the diffusion of nanoparticles is inversely proportional to their size [60,61], a good spreading of loaded nanoparticles within the agar matrix was anticipated. At 25 °C, unloaded HAMA/CS-Xlinked nanoparticles had no antibacterial effect, but BC-loaded nanoparticles were effective against *S. aureus* (Fig. 5A, Table 2). Plates inoculated with *S. aureus*, *MRSA*, and *S. epidermidis* showed a clear inhibition zone around the positive control containing BC solution after incubation at



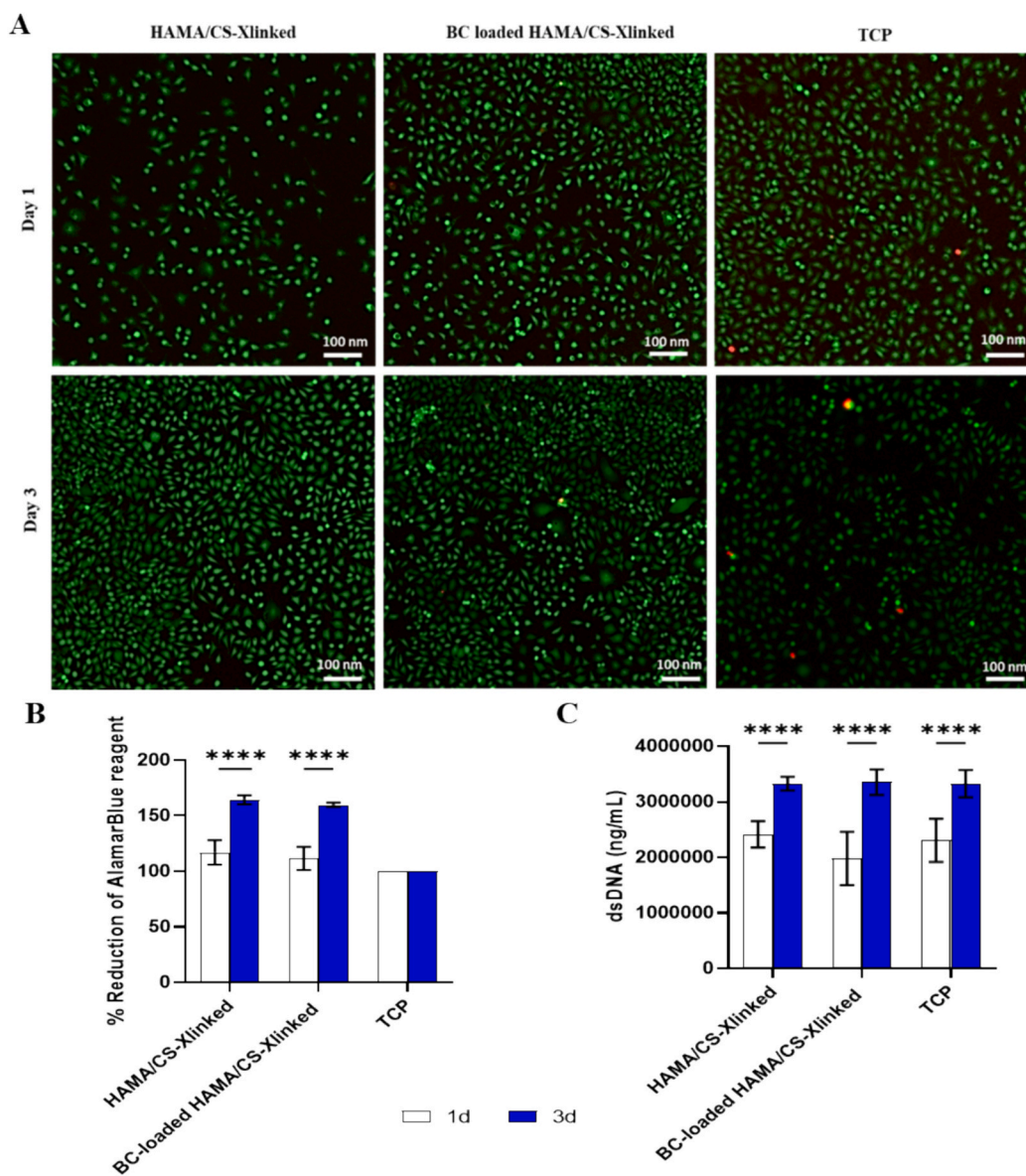


**Fig. 8.** (A) Representative fluorescent images of live (green)/dead (red) cells on the HAMA/CS-Xlinked and the BC-loaded HAMA/CS-Xlinked nanoparticles. Scale bar is 100  $\mu$ m. (B) Metabolic activity of L929 cells cultured with the HAMA/CS-Xlinked and the BC-loaded HAMA/CS-Xlinked nanoparticles determined by Alamar blue assay. (C) Double strand DNA (dsDNA) quantification assay of L929 cells cultured with the HAMA/CS-Xlinked and the BC-loaded HAMA/CS-Xlinked nanoparticles, after 1 day and 3 days. L929 cells in tissue culture plastic (TCP) were used as a positive control. Significant differences: \*\*\*\* $p$  < 0.0001.

25 °C.

When incubated at 37 °C, the loaded nanoparticles had an antibacterial effect against all studied strains, as evidenced by the clear inhibition zone formed on all tested bacteria cultures (between 11 and 15 mm in diameter) (Fig. 5B, Table 2).

Although the BC-loaded HAMA/CS-Xlinked nanoparticles showed a lower inhibition effect at 25 °C, the results suggest that this formulation can be used in a variety of strategies to prevent the proliferation of the most common microorganisms responsible for wound infection [66,67]. The encapsulation of BC is advantageous for its administration since its effects would be stronger when in direct contact with the wound bed, at temperatures closer to 37 °C.

The effect of the BC-loaded HAMA/CS-Xlinked nanoparticles on bacterial viability was evaluated (Fig. 6). The results show that the BC-loaded HAMA/CS-Xlinked nanoparticles had a bacterial inhibitory effect for all strains after 24 h incubation (Fig. 6). The same trend was observed in the bacteria treated with BC in solution (Fig. 6). As for the HAMA/CS-Xlinked nanoparticles, they had no effect on the bacterial

growth, demonstrating a similar pattern to the bacterial controls without any treatment. The HAMA/CS-Xlinked nanoparticles exhibited no impact on bacterial growth, displaying a comparable trend to the untreated bacterial controls. Following a 72 h incubation period, a similar pattern was seen, suggesting that the HAMA/CS-linked nanoparticles loaded with BC exhibit a potent antibacterial activity.

The antibiofilm potential of the BC-loaded HAMA/CS-Xlinked nanoparticles was also evaluated using the microtiter plate method (Fig. 7A). Following incubation periods of 24 h and 72 h, the results indicate that no viable bacteria were detected when exposed to the BC-loaded HAMA/CS-Xlinked nanoparticles. However, the growth and production of biofilm were not affected by HAMA/CS-Xlinked nanoparticles or BC in solution, indicating that they did not hinder these processes. Similar patterns were seen in relation to the biofilm biomass, as depicted in Fig. 7B. The results suggest that the BC-loaded HAMA/CS-Xlinked nanoparticles reduced the amount of biofilm after 24 h and 72 h of incubation, in comparison to the bacteria treated with HAMA/CS-Xlinked nanoparticles and those that received no treatment. This

behaviour was observed for all the bacteria that were examined.

The cytotoxic response to the BC-loaded HAMA/CS-Xlinked and HAMA/CS-Xlinked nanoparticles was evaluated using L929. The live/dead assay (Fig. 8A) showed a minimal number of dead cells (in red), evidencing no cytotoxic effect. Significant increase of the metabolic activity of cells cultured on BC loaded and unloaded HAMA/CS-Xlinked nanoparticles were observed on the third day: L929 cultured on BC-loaded HAMA/CS-Xlinked and HAMA/CS-Xlinked nanoparticles had the similar metabolic activity (Fig. 8B). An increase in DNA content and metabolic activity was observed over time in culture, indicating that the nanoparticles sustained cell proliferation (Fig. 8C).

This antibacterial study showed that BC-loaded HAMA/CS-Xlinked nanoparticles potential for treating wound infections. These nanoparticles effectively inhibit bacterial growth and prevent biofilm formation, while also promoting cellular growth and proliferation. They can serve as beneficial alternatives for existing conventional topical treatments, delivering antibiotics directly to deep infected wounds [68].

#### 4. Conclusions

This work demonstrated the successful production of CS/HAMA nanoparticles for the delivery of BC. The nanoparticles were produced using, for the first time, methacrylated HA that allows photo-crosslink upon UV irradiation. Cross-linked nanoparticles were smaller and more homogeneous when loaded with BC. The obtained nanoparticles are promising as topical antibacterial compounds for wound treatments the antibiotic-loaded nanoparticles inhibited the growth of bacterial strains common in diabetic foot ulcers. The proposed methodology is simple, versatile and scalable for industrial production of nanoparticles. The process is both sustainable and cost-effective, as it uses building blocks from renewable sources and does not require specialized equipment or aggressive temperatures or solvent conditions. Furthermore, these nanoparticles demonstrate enhanced antibacterial and antibiofilm effects and are non-cytotoxic on fibroblasts. While a comparison with other wound healing therapies was not contemplated, the efficacy of the proposed system can be tested against *in vitro* and *in vivo* models in future experiments to assess clinical applicability. The focus is envisaged to be on chronic wound therapies, as these wounds are challenging to treat and are often associated with underlying complications prevalent in modern societies.

#### CRedit authorship contribution statement

**Raquel R. Gonçalves:** Writing – original draft, Formal analysis, Data curation, Conceptualization. **Daniela Peixoto:** Writing – review & editing, Validation, Supervision, Software, Methodology, Conceptualization. **Rui R. Costa:** Writing – review & editing, Supervision, Methodology, Investigation. **Albina R. Franco:** Validation, Software, Methodology, Investigation. **Vânia I.B. Castro:** Formal analysis, Data curation. **Ricardo A. Pires:** Formal analysis, Data curation. **Rui L. Reis:** Resources. **Iva Pashkuleva:** Writing – review & editing, Validation, Supervision, Resources. **Devid Maniglio:** Writing – review & editing. **Annalisa Tirella:** Writing – review & editing, Validation, Supervision. **Antonella Motta:** Writing – review & editing, Validation, Supervision. **Nátalia M. Alves:** Writing – review & editing, Validation, Supervision, Resources, Project administration.

#### Declaration of competing interest

The authors declare that they have no known competing financial interests or personal relationships that could have appeared to influence the work reported in this paper.

#### Data availability

Data will be made available on request.

#### Acknowledgements

The authors acknowledge the financial support of the European Commission through project APTADEGRAD (HORIZON-EIC-2022-PATHFINDEROPEN-01-101099063) and SHIFT Project (funded by the European Union's Horizon 2020 Research and Innovation programme under the Maria Skłodowska-Curie grant agreement no. 101008041). R. R.G. acknowledges the Erasmus Program for the travel grant to the University of Trento. R.R.C. acknowledges FCT for support through grant 2022.00764.CEECIND/CP1718/CT0020 (<https://doi.org/10.54499/2022.00764.CEECIND/CP1718/CT0020>). A.R.F. acknowledges FCT for support through grant DL 57/2016/CP1377/CT0054 (<https://doi.org/10.54499/DL57/2016/CP1377/CT0054>) and PTDC/BTM-MAT/2844/2021 (<https://doi.org/10.54499/PTDC/BTM-MAT/2844/2021>) funded by the Portuguese National Science Foundation (FCT) through OE component. The authors would like to thank the contributions to this research from the project "TERM RES Hub – Scientific Infrastructure for Tissue Engineering and Regenerative Medicine", reference PINFRA/22190/2016 (Norte-01-0145-FEDER-022190), funded by the Portuguese National Science Foundation (FCT) in cooperation with the Northern Portugal Regional Coordination and Development Commission (CCDR-N), for providing relevant lab facilities, state-of-the art equipment and highly qualified human resources.

#### Appendix A. Supplementary data

Supplementary data to this article can be found online at <https://doi.org/10.1016/j.ijbiomac.2024.134250>.

#### References

- [1] R.G. Frykberg, J. Banks, Challenges in the treatment of chronic wounds, *Adv Wound Care (New Rochelle)* 4 (2015) 560–582, <https://doi.org/10.1089/wound.2015.0635>.
- [2] G. Broughton, J.E. Janis, C.E. Attinger, The basic science of wound healing, *Plast. Reconstr. Surg.* 117 (2006), <https://doi.org/10.1097/01.prs.0000225430.42531.c2>.
- [3] R.G. Frykberg, J. Banks, Challenges in the treatment of chronic wounds, *Adv Wound Care (New Rochelle)* 4 (2015) 560–582, <https://doi.org/10.1089/wound.2015.0635>.
- [4] S. Guo, L.A. DiPietro, Critical review in oral biology & medicine: factors affecting wound healing, *J. Dent. Res.* 89 (2010) 219–229, <https://doi.org/10.1177/0022034509359125>.
- [5] C.K. Sen, G.M. Gordillo, S. Roy, R. Kirsner, L. Lambert, T.K. Hunt, F. Gottrup, G. C. Gurtner, M.T. Longaker, Human skin wounds: a major and snowballing threat to public health and the economy: PERSPECTIVE ARTICLE, *Wound Repair Regen.* 17 (2009) 763–771, <https://doi.org/10.1111/j.1524-475X.2009.00543.x>.
- [6] M. Holl, J. Kowalewski, C. Zimek, Z. Fiedor, P. Kaminski, A. Oldak, T. Moniuszko, Chronic diabetic wounds and their treatment with skin substitutes, *Cells* 10 (2021) doi:10.3390/cells10030655.
- [7] A. Alavi, R.G. Sibbald, D. Mayer, L. Goodman, M. Botros, D.G. Armstrong, K. Woo, T. Boeni, E.A. Ayello, R.S. Kirsner, Diabetic foot ulcers: part II. Management, *J Am Acad Dermatol* 70 (2014), <https://doi.org/10.1016/j.jaad.2013.07.048>, 21.e1-21.e24.
- [8] R. Stein-Wexler, *Musculoskeletal Infection*, 2015, [https://doi.org/10.1007/978-3-642-45381-6\\_19](https://doi.org/10.1007/978-3-642-45381-6_19).
- [9] F. Gottrup, A specialized wound-healing center concept: importance of a multidisciplinary department structure and surgical treatment facilities in the treatment of chronic wounds, *Am. J. Surg.* 187 (2004) S38–S43, [https://doi.org/10.1016/S0002-9610\(03\)00303-9](https://doi.org/10.1016/S0002-9610(03)00303-9).
- [10] K. Järbrink, G. Ni, H. Sönnergren, A. Schmidtchen, C. Pang, R. Bajpai, J. Car, Prevalence and incidence of chronic wounds and related complications: a protocol for a systematic review, *Syst. Rev.* 5 (2016) 1–6, <https://doi.org/10.1186/s13643-016-0329-y>.
- [11] J. Tan, S. Shah, A. Thomas, H.D. Ou-Yang, Y. Liu, The influence of size, shape and vessel geometry on nanoparticle distribution, *Microfluid Nanofluidics* 14 (2013) 77–87, <https://doi.org/10.1007/s10404-012-1024-5>.
- [12] J.W. Hickey, J.L. Santos, J.M. Williford, H.Q. Mao, Control of polymeric nanoparticle size to improve therapeutic delivery, *J. Control. Release* 219 (2015) 536–547, <https://doi.org/10.1016/j.jconrel.2015.10.006>.
- [13] M.J. Mitchell, M.M. Billingsley, R.M. Haley, M.E. Wechsler, N.A. Peppas, R. Langer, Engineering precision nanoparticles for drug delivery, *Nat. Rev. Drug Discov.* 20 (2021) 101–124, <https://doi.org/10.1038/s41573-020-0090-8>.
- [14] R.R. Costa, R.L. Reis, I. Pashkuleva, Glycosaminoglycans as polyelectrolytes: implications in bioactivity and assembly of biomedical devices, *Int. Mater. Rev.* 67 (2022) 765–795, <https://doi.org/10.1080/09506608.2022.2026860>.

- [15] I. Aranaz, A.R. Alcántara, M.C. Civera, C. Arias, B. Elorza, A.H. Caballero, N. Acosta, Chitosan: an overview of its properties and applications, *Polymers (Basel)* 13 (2021), <https://doi.org/10.3390/polym13193256>.
- [16] N. Morin-crimi, E. Lichtfouse, G. Torri, G. Crini, N. Morin-crimi, E. Lichtfouse, G. Torri, G.C. Fundamentals, N. Morin-crimi, E. Lichtfouse, G. Torri, G. Crini, Fundamentals and Applications of Chitosan to Cite this Version: HAL Id: hal-02152878 Fundamentals and Applications of Chitosan, Springer International Publishing AG, 2019.
- [17] W. Xia, P. Liu, J. Zhang, J. Chen, Biological activities of chitosan and chitooligosaccharides, *Food Hydrocoll.* 25 (2011) 170–179, <https://doi.org/10.1016/j.foodhyd.2010.03.003>.
- [18] S. Gabriel Kou, L. Peters, M. Mucalo, Chitosan: a review of molecular structure, bioactivities and interactions with the human body and micro-organisms, *Carbohydr. Polym.* 282 (2022) 119132, <https://doi.org/10.1016/j.carbpol.2022.119132>.
- [19] A. Fallacara, E. Baldini, S. Manfredini, S. Vertuani, Hyaluronic acid in the third millennium, *Polymers (Basel)* 10 (2018), <https://doi.org/10.3390/polym10070701>.
- [20] A. Yasin, Y. Ren, J. Li, Y. Sheng, C. Cao, K. Zhang, Advances in hyaluronic acid for biomedical applications 10 (2022) 1–12, <https://doi.org/10.3389/fbioe.2022.910290>.
- [21] Y. Parajó, I. D'Angelo, A. Welle, M. Garcia-Fuentes, M.J. Alonso, Hyaluronic acid/chitosan nanoparticles as delivery vehicles for VEGF and PDGF-BB, *Drug Deliv.* 17 (2010) 596–604, <https://doi.org/10.3109/10717544.2010.509357>.
- [22] A. Tirella, K. Kloc-Muniak, L. Good, J. Ridde, M. Ashford, S. Puri, N. Tirelli, CD44 targeted delivery of siRNA by using HA-decorated nanotechnologies for KRAS silencing in cancer treatment, *Int. J. Pharm.* 561 (2019) 114–123, <https://doi.org/10.1016/j.ijpharm.2019.02.032>.
- [23] E. Lallana, J.M. Rios De La Rosa, A. Tirella, M. Pelliccia, A. Gennari, L.J. Stratford, S. Puri, M. Ashford, N. Tirelli, Chitosan/hyaluronic acid nanoparticles: rational design revisited for RNA delivery, *Mol. Pharm.* 14 (2017) 2422–2436, <https://doi.org/10.1021/acs.molpharmaceut.7b00320>.
- [24] L. Yang, S. Gao, S. Asghar, G. Liu, J. Song, X. Wang, Q. Ping, C. Zhang, Y. Xiao, Hyaluronic acid/chitosan nanoparticles for delivery of curcuminoid and its in vitro evaluation in glioma cells, *Int. J. Biol. Macromol.* 72 (2015) 1391–1401, <https://doi.org/10.1016/j.ijbiomac.2014.10.039>.
- [25] A.C. Lima, R.L. Reis, H. Ferreira, N.M. Neves, Cellular uptake of three different nanoparticles in an inflammatory arthritis scenario versus Normal conditions, *Mol. Pharm.* 18 (2021) 3235–3246, <https://doi.org/10.1021/acs.molpharmaceut.1c00066>.
- [26] O.Z. Fisher, N.A. Peppas, Polybasic nanomatrices prepared by UV-initiated photopolymerization, *Macromolecules* 42 (2009) 3391–3398, <https://doi.org/10.1021/ma801966r>.
- [27] D.C. Forbes, N.A. Peppas, Polycationic nanoparticles for siRNA delivery: comparing ARGENT ATRP and UV-initiated formulations, *ACS Nano* 8 (2014) 2908–2917, <https://doi.org/10.1021/nn500101c>.
- [28] S. Maiz-Fernández, L. Pérez-Álvarez, U. Silván, J.L. Vilas-Vilela, S. Lanceros-Mendez, Photocrosslinkable and self-healable hydrogels of chitosan and hyaluronic acid, *Int. J. Biol. Macromol.* 216 (2022) 291–302, <https://doi.org/10.1016/j.ijbiomac.2022.07.004>.
- [29] S. Maiz-Fernández, N. Barroso, L. Pérez-Álvarez, U. Silván, J.L. Vilas-Vilela, S. Lanceros-Mendez, 3D printable self-healing hyaluronic acid/chitosan polycomplex hydrogels with drug release capability, *Int. J. Biol. Macromol.* 188 (2021) 820–832, <https://doi.org/10.1016/j.ijbiomac.2021.08.022>.
- [30] O.Z. Fisher, T. Kim, S.R. Dietz, N.A. Peppas, Enhanced core hydrophobicity, functionalization and cell penetration of polybasic nanomatrices, *Pharm. Res.* 26 (2009) 51–60, <https://doi.org/10.1007/s11095-008-9704-2>.
- [31] E. Tous, J.L. Ifkovits, K.J. Koomalsingh, T. Shuto, T. Soeda, N. Kondo, J.H. Gorman, R.C. Gorman, J.A. Burdick, Influence of injectable hyaluronic acid hydrogel degradation behavior on infarction-induced ventricular remodeling, *Biomacromolecules* 12 (2011) 4127–4135, <https://doi.org/10.1021/bm201198x>.
- [32] R. Nguyen, N.R. Khanna, A.O. Safadi, Y. Sun, *Bacitracin Topical*, 2022.
- [33] C. Loebel, C.B. Rodell, M.H. Chen, J.A. Burdick, Therapeutics and for 3D-printing 12 (2020) 1521–1541, <https://doi.org/10.1038/nprot.2017.053.Shear-thinning>.
- [34] E. Lallana, J.M. Rios De La Rosa, A. Tirella, M. Pelliccia, A. Gennari, L.J. Stratford, S. Puri, M. Ashford, N. Tirelli, Chitosan/hyaluronic acid nanoparticles: rational design revisited for RNA delivery, *Mol. Pharm.* 14 (2017) 2422–2436, <https://doi.org/10.1021/acs.molpharmaceut.7b00320>.
- [35] L. Othman, A. Sleiman, R.M. Abdel-Massih, Antimicrobial activity of polyphenols and alkaloids in middle eastern plants, *Front. Microbiol.* 10 (2019), <https://doi.org/10.3389/fmicb.2019.00911>.
- [36] C. Luo, M. Chen, K. Luo, X. Yin, M.M. Onchari, X. Wang, J. Zhang, H. Zhong, B. Tian, Genome sequencing and genetic engineering reveal the contribution of bacitracin produced by *Bacillus paralicheniformis* CPL618 to anti-*Staphylococcus aureus* activity, *Curr. Microbiol.* 80 (2023), <https://doi.org/10.1007/s00284-023-03196-1>.
- [37] Allison L. King, Significance of Open Wounds Potentially Caused by Non-Lethal Weapons, 2019 <https://www.researchgate.net/publication/337926082>.
- [38] L. Othman, A. Sleiman, R.M. Abdel-Massih, Antimicrobial activity of polyphenols and alkaloids in middle eastern plants, *Front. Microbiol.* 10 (2019), <https://doi.org/10.3389/fmicb.2019.00911>.
- [39] KnowledgeBASE The antimicrobial index, Bacitracin (Baci-IM), (n.d.). <https://antibiotics.toku-e.com/antimicrobial367.1.html>.
- [40] M. Bubonja-Sonje, S. Knezević, M. Abram, Challenges to antimicrobial susceptibility testing of plant-derived polyphenolic compounds, *Arh. Hig. Rada Toksikol.* 71 (2020) 300–311, <https://doi.org/10.2478/aiht-2020-71-3396>.
- [41] C. Valgas, S. Machado De Souza Elza, F.A. Smânia, A. Smânia, Screening methods to determine antibacterial activity of natural products, *Braz. J. Microbiol.* 38 (2007) 369–380.
- [42] S. Zheng, M. Bawazir, A. Dhall, H.E. Kim, L. He, J. Heo, G. Hwang, Implication of surface properties, bacterial motility, and hydrodynamic conditions on bacterial surface sensing and their initial adhesion, *Front. Bioeng. Biotechnol.* 9 (2021), <https://doi.org/10.3389/fbioe.2021.643722>.
- [43] A.R. Franco, E. Palma Kimmerling, C. Silva, F.J. Rodrigues, I.B. Leonor, R.L. Reis, D.L. Kaplan, Silk-based antimicrobial polymers as a new platform to design drug-free materials to impede microbial infections, *Macromol. Biosci.* 18 (2018) 1–15, <https://doi.org/10.1002/mabi.201800262>.
- [44] J. Hudzicki, Kirby-Bauer disk diffusion susceptibility test protocol author information, *American Society For Microbiology* (2012) 1–13.
- [45] A.R. Franco, E. Palma Kimmerling, C. Silva, F.J. Rodrigues, I.B. Leonor, R.L. Reis, D.L. Kaplan, Silk-based antimicrobial polymers as a new platform to design drug-free materials to impede microbial infections, *Macromol. Biosci.* 18 (2018), <https://doi.org/10.1002/mabi.201800262>.
- [46] E.F. Haney, M.J. Trimble, R.E.W. Hancock, Microtiter plate assays to assess antibiofilm activity against bacteria, *Nat. Protoc.* 16 (2021) 2615–2632, <https://doi.org/10.1038/s41596-021-00515-3>.
- [47] C. Correia, R.O. Sousa, A.C. Vale, D. Peixoto, T.H. Silva, R.L. Reis, I. Pashkuleva, N.M. Alves, Adhesive and biodegradable membranes made of sustainable catechol-functionalized marine collagen and chitosan, *Colloids Surf. B Biointerfaces* 213 (2022), <https://doi.org/10.1016/j.colsurfb.2022.112409>.
- [48] C. Correia, D.S. Da Costa, A.R. Inácio, A.C. Vale, D. Peixoto, T.H. Silva, R.L. Reis, I. Pashkuleva, N.M. Alves, Adhesive and antibacterial films based on marine-derived fucoïdan and chitosan, *ACS Sustain. Chem. Eng.* 10 (2022) 16770–16779, <https://doi.org/10.1021/acssuschemeng.2c05144>.
- [49] S. Gimondi, R.L. Reis, H. Ferreira, N.M. Neves, Microfluidic-driven mixing of high molecular weight polymeric complexes for precise nanoparticle downsizing, *Nanomedicine* 43 (2022), <https://doi.org/10.1016/j.nano.2022.102560>.
- [50] I. Serrano-Sevilla, Á. Artiga, S.G. Mitchell, L. De Matteis, J.M. de la Fuente, Natural polysaccharides for siRNA delivery: Nanocarriers based on chitosan, hyaluronic acid, and their derivatives, *Molecules* 24 (2019), <https://doi.org/10.3390/molecules24142570>.
- [51] K.N. Clayton, J.W. Salameh, S.T. Wereley, T.L. Kinzer-Ursem, Physical characterization of nanoparticle size and surface modification using particle scattering diffusometry, *Biomicrofluidics* 10 (2016) 1–14, <https://doi.org/10.1063/1.4962992>.
- [52] S. Boddohi, N. Moore, P.A. Johnson, M.J. Kipper, Polysaccharide-based polyelectrolyte complex nanoparticles from chitosan, heparin, and hyaluronan, (2009) 1402–1409.
- [53] Y. Agrawal, V. Patel, Nanosuspension: an approach to enhance solubility of drugs, *J. Adv. Pharm. Technol. Res.* 2 (2011) 81, <https://doi.org/10.4103/2231-4040.82950>.
- [54] H.T. Phan, A.J. Haes, What does nanoparticle stability mean? HHS Public Access, *J Phys Chem C Nanomater Interfaces* 123 (2019) 16495–16507, <https://doi.org/10.1021/acs.jpcc.9b00913.What>.
- [55] S.L. Percival, S. McCarty, J.A. Hunt, E.J. Woods, The effects of pH on wound healing, biofilms, and antimicrobial efficacy, *Wound Repair Regen.* 22 (2014) 174–186, <https://doi.org/10.1111/wrr.12125>.
- [56] B. Nagoba, A. Gavkare, A. Rayate, S. Mumbre, A. Rao, B. Warad, N. Nanaware, N. Jamadar, Role of an acidic environment in the treatment of diabetic foot infections: a review, *World J. Diabetes* 12 (2021) 1539–1549, <https://doi.org/10.4239/wjdv.v12.i9.1539>.
- [57] P. Sim, X.L. Strudwick, Y.M. Song, A.J. Cowin, S. Garg, Influence of acidic pH on wound healing in vivo: a novel Perspective for wound treatment, *Int. J. Mol. Sci.* 23 (2022), <https://doi.org/10.3390/ijms232113655>.
- [58] D.G. Metcalf, M. Haalboom, P.G. Bowler, C. Gamerith, E. Sigl, A. Heinze, M.W. M. Burnet, Elevated wound fluid pH correlates with increased risk of wound infection, *Wound Medicine* 26 (2019), <https://doi.org/10.1016/j.wndm.2019.100166>.
- [59] R. Strohal, M. Mittlbö, G. Hä, The Management of Critically Colonized and Locally Infected Leg Ulcers with an Acid-Oxidizing Solution: A Pilot Study, n.d.
- [60] J. Tan, S. Shah, A. Thomas, H.D. Ou-Yang, Y. Liu, The influence of size, shape and vessel geometry on nanoparticle distribution, *Microfluid. Nanofluid.* 14 (2013) 77–87, <https://doi.org/10.1007/s10404-012-1024-5>.
- [61] J.W. Hickey, J.L. Santos, J.M. Williford, H.Q. Mao, Control of polymeric nanoparticle size to improve therapeutic delivery, *J. Control. Release* 219 (2015) 536–547, <https://doi.org/10.1016/j.jconrel.2015.10.006>.
- [62] D.M. Ibeogu, A. Boussahel, S. Cragg, J. Tsiouklis, E. Barbu, Nanoparticles of alkylglyceryl dextran and poly(ethyl cyanoacrylate) for applications in drug delivery: preparation and characterization, *Journal of Polymeric Materials and Polymeric Biomaterials* 66 (2017) 265–279, <https://doi.org/10.1080/00914037.2016.1201827>.
- [63] D.S. Nikam, S.V. Jadhav, V.M. Khot, R.S. Ningthoujam, C.K. Hong, S.S. Mali, S. H. Pawar, Colloidal stability of polyethylene glycol functionalized Co<sub>0.5</sub>N<sub>0.5</sub>Fe<sub>2</sub>O<sub>4</sub> nanoparticles: effect of pH, sample and salt concentration for hyperthermia application, *RSC Adv.* 4 (2014) 12662–12671, <https://doi.org/10.1039/c3ra47319h>.
- [64] J.C. Dumville, B.A. Lipsky, C. Hoey, M. Cruciani, M. Fisco, J. Xia, Topical antimicrobial agents for treating foot ulcers in people with diabetes, *Cochrane Database Syst. Rev.* 2017 (2017), <https://doi.org/10.1002/14651858.CD011038.pub2>.
- [65] S. Rittenhouse, S. Biswas, J. Broskey, L. McCloskey, T. Moore, S. Vasey, J. West, M. Zalacain, R. Zonis, D. Payne, Selection of retapamulin, a novel pleuromutilin for

- topical use, *Antimicrob. Agents Chemother.* 50 (2006) 3882–3885, <https://doi.org/10.1128/AAC.00178-06>.
- [66] M. Stańkowska, K. Garbacz, A. Korzon-Burakowska, M. Bronk, M. Skotarczak, A. Szymańska-Dubowik, Microbiological, clinical and radiological aspects of diabetic foot ulcers infected with methicillin-resistant and-sensitive *Staphylococcus aureus*, *Pathogens* 11 (2022), <https://doi.org/10.3390/pathogens11060701>.
- [67] H. Galkowska, A. Podbielska, W.L. Olszewski, E. Stelmach, M. Luczak, G. Rosinski, W. Karnafel, Epidemiology and prevalence of methicillin-resistant *Staphylococcus aureus* and *Staphylococcus epidermidis* in patients with diabetic foot ulcers: focus on the differences between species isolated from individuals with ischemic vs. neuropathic foot ulcers, *Diabetes Res. Clin. Pract.* 84 (2009) 187–193, <https://doi.org/10.1016/j.diabres.2009.02.008>.
- [68] P. Dam, M. Celik, M. Ustun, S. Saha, C. Saha, E.A. Kacar, S. Kugu, E.N. Karagulle, S. Tasoglu, F. Buyukserin, R. Mondal, P. Roy, M.L.R. Macedo, O.L. Franco, M. H. Cardoso, S. Altuntas, A.K. Mandal, Wound healing strategies based on nanoparticles incorporated in hydrogel wound patches, *RSC Adv.* 13 (2023) 21345–21364, <https://doi.org/10.1039/d3ra03477a>.